The Astrophysical Journal, 973:27 (13pp), 2024 September 20 https://doi.org/10.3847/1538-4357/ad631e
© 2024. The Author(s). Published by the American Astronomical Society.
OPEN ACCESS

Flat Spectra of Energetic Particles in Interplanetary Shock Precursors

Mikhail Malkov[1], Joe Giacalone[2], and Fan Guo[3]
[1] Department of Astronomy and Astrophysics, University of California, San Diego, La Jolla, CA 92093, USA
[2] Lunar & Planetary Laboratory, University of Arizona, Tucson, AZ 85721, USA
[3] Los Alamos National Laboratory, Los Alamos, NM 87545, USA
Received 2024 January 17; revised 2024 June 16; accepted 2024 July 11; published 2024 September 12

Abstract

The observed energy spectra of accelerated particles at interplanetary shocks often do not match the diffusive shock acceleration (DSA) theory predictions. In some cases, the particle flux forms a plateau over a wide range of energies, extending *upstream of the shock* for up to seven flux *e*-folds before submerging into the background spectrum. Remarkably, at and downstream of the shock we have studied in detail, the flux falls off in energy as ϵ^{-1}, consistent with the DSA prediction for a strong shock. The upstream plateau suggests a particle transport mechanism different from those traditionally employed in DSA models. We show that a standard (linear) DSA solution based on a widely accepted diffusive particle transport with an underlying resonant wave–particle interaction is inconsistent with the plateau in the particle flux. To resolve this contradiction, we modify the DSA theory in two ways. First, we include a dependence of the particle diffusivity κ on the particle flux F (nonlinear particle transport). Second, we invoke short-scale magnetic perturbations that are self-consistently generated by, but not resonant with, accelerated particles. They lead to the particle diffusivity increasing with the particle energy as $\propto\epsilon^{3/2}$ that simultaneously decreases with the particle flux as $1/F$. The combination of these two trends results in the flat spectrum upstream. We speculate that nonmonotonic spatial variations of the upstream spectrum, apart from being time-dependent, may also result from non-DSA acceleration mechanisms at work upstream, such as stochastic Fermi or magnetic pumping acceleration.

Unified Astronomy Thesaurus concepts: Interplanetary shocks (829); Interplanetary particle acceleration (826)

1. Introduction

Diffusive shock acceleration (DSA; Krymskii 1977; Axford et al. 1978; Bell 1978; Blandford & Ostriker 1978) is arguably the most universal and robust mechanism whereby particles can be accelerated to high energies in shocks across the Universe. Its physical and intuitive grounds are comprehensible. The particle momentum spectrum behind the shock comes from a "back-of-the-envelope" calculation. It is a power law $\propto p^{-q}$, with an index $q = 3r/(r-1)$ that, to the first approximation, depends only on the shock compression r.

The simplicity of the DSA is, however, deceptive. After almost half a century of research, it is still challenging to calculate the rate at which it operates and the maximum energy particles can gain in realistic shock environments. Its index q often disagrees with observations even if the shock is known to be strong, and the index q should be equal to 4. When the spectrum is harder than predicted, the difference is usually explained by a nonlinear shock modification due to the growing pressure of accelerated particles (see Malkov & Drury 2001 for a review). When softer, the disagreement can, e.g., be attributed to the nonstationarity and curvature of the shock, strong short-scale magnetic perturbations generated by accelerated particles, and propagation of particle scattering waves relative to the plasma flow (Kennel et al. 1986; Bell et al. 2019; Hanusch et al. 2019; Malkov & Aharonian 2019; Diesing & Caprioli 2021). These arguments are primarily applied to the supernova remnant shocks, in which measurements of energetic particles are limited in accuracy and indirect by nature, thus obscuring the cause of the spectral softening. The particle spectra are inferred from the emission of accelerated electrons and, maybe, from the γ- radiation generated by accelerated protons interacting with adjacent molecular clouds, if present. If so, telling the radiatively more efficient leptons from overwhelmingly more abundant hadrons is still challenging.

This paper considers an even more puzzling DSA disagreement with the observed spectra. Notably, at some, but not all, interplanetary shocks observed in situ (e.g., Lario et al. 2018, 2022; Perri et al. 2023), the particle flux *flattens upstream,* whereas the downstream part still agrees with the DSA. Since the disagreement is partial, it helps identify the DSA elements responsible. In addition, it might shed light on how the DSA is sped up by waves excited by the accelerated particles themselves (Bell 1978). Recall that within the DSA, particles gain energy when they cross and recross the shock by scattering off magnetic perturbations of whatever origin. Therefore, strong self-generated waves "bootstrap" the particle acceleration.

Central to the bootstrap is a simultaneous growth of wave amplitudes and their lengths during the acceleration. Scattering is most efficient when the wave–particle resonance condition, $kr_g(p) \sim 1$, is maintained throughout the wave and particle spectra up to at least the maximum particle momentum, $p_{\max}$. Here, r_g is the particle gyroradius, $r_g = cp/eB_0$, and k is the wavenumber of resonant Alfvén waves. However, the fastest-growing waves do not necessarily scatter particles most rapidly, which is required for efficient acceleration.

Resonant waves typically saturate at a level not significantly higher than $\delta B/B_0 \sim 1$ (Völk et al. 1984). Macroscopically driven nonresonant instabilities may continue to grow beyond this level. Two types of them are often invoked in DSA

Original content from this work may be used under the terms of the Creative Commons Attribution 4.0 licence. Any further distribution of this work must maintain attribution to the author(s) and the title of the work, journal citation and DOI.

treatments. One is current-driven, also called the Bell's instability (Bell 2004). The other one is an acoustic instability driven by the pressure gradient of accelerated particles (Drury & Falle 1986). Because they are powered by these macroscopic sources of free energy, nonresonantly driven waves act differently on energetic particles than resonantly driven waves. In the latter case, a wave with a given wavenumber k interacts only with a narrow group of particles in momentum space. Instead, nonresonantly driven waves indiscriminately affect broader swaths of energetic particles.

We will show that a *nonresonant* wave–particle interaction also leads to a different scaling of particle diffusivity with their energy. As a result, their propagation into the upstream medium against the inflowing plasma becomes energy-independent beyond a certain distance upstream, thus flattening the spectrum. Hence, it is expected to occur when the upstream population of energetic particles grows to the point beyond which the nonresonantly driven instabilities dominate the resonantly driven ion-cyclotron instability. We will also show that this change of the particle transport regime upstream does not affect the DSA-predicted spectral slope downstream, as also observed. The question of when exactly this change of instability occurs depends on the strength and type of the nonresonant drivers (current, pressure gradients, and pressure anisotropy, leading to the firehose and mirror-type plasma instabilities; Malkov et al. 2010; Bykov et al. 2013).

The goal of this paper is to demonstrate that the mechanism outlined above may indeed flatten the upstream spectrum. We will use just one highly representative shock observed in 2005 May that generated nearly perfectly flat spectra in a broad energy range. At the same time, considering just one case does not suffice to derive general conditions under which the shock flattening occurs. Apart from the strength of the instability driver, they depend on other shock parameters discussed in the above references and on the shock geometry. The latter controls the shock's ability to sustain an intense population of accelerated particles upstream against losses. Understanding the general conditions for spectral flattening clearly requires a separate survey-type study with detailed knowledge of the parameters of each shock in the sample. It will be particularly critical to differentiate between the resonant and nonresonant cases. However, such a study is out of the scope of the present paper.

We have organized this paper along its line of arguments as follows. Because the flat upstream spectra are uncommon, in the next section, we specify particle transport regimes that may result in such spectra. Next, we review the turbulence spectra that may be consistent with such regimes. Each of these two steps will be made assuming two different types of wave–particle interaction: resonant and nonresonant. The above-described analyses will allow us to eliminate some common combinations of turbulence spectra, particle transport regimes, and wave–particle interaction types (resonant versus nonresonant) inconsistent with the flat spectra. In Section 2.2, we show that the wave–particle interaction is likely nonresonant, the particle transport must be nonlinear (flux-dependent), and the wave spectrum is likely to be of the Iroshnikov–Kraichnan type. In Section 3, we discuss a nonlinear transport regime that leads to the flat spectra. Section 4 deals with the acceleration model based on this transport regime. In Section 5, we fit the model predictions to the data. The paper concludes with a summary and discussion of its results.

2. Observational Hints

In this section, we constrain the particle transport and its underlying MHD turbulence required for the spectral flattening observed at the interplanetary shock of 2005 May (e.g., Lario et al. 2018, 2022; Perri et al. 2023). We selected this data set because the flat particle flux upstream, inconsistent with the DSA, coexists with its DSA-compliant downstream counterpart. This example offers insights into conditions under which the "standard" (linear diffusion) DSA model fails. It helps eliminate turbulence and transport combinations inconsistent with the data. We will show that if the particle diffusivity does not depend on their intensity, it is difficult to explain the flat particle flux. We will, therefore, introduce such a dependence in a way similar to that proposed at the inception of the DSA (Bell 1978). We will also rule out several types of turbulence spectra. These analyses help us zero in on a unique combination of turbulence and particle transport regimes leading to the flat particle flux upstream of the shock.

2.1. Constraining the Particle Diffusion Coefficient

Figure 1 demonstrates disagreements with the "standard" DSA model. However, we start with what is agreeable. On the downstream side, the particle flux decreases approximately as ϵ^{-1} with energy, consistent with the DSA prediction for a shock with a compression ratio close to 4. Immediately on the upstream side, the low-energy part of the spectrum initially decays more steeply with distance from the shock. This behavior is also *qualitatively* consistent with the DSA if the particle diffusivity grows with energy.

Further upstream, the disagreements with the DSA become obvious. Let us consider a general steady-state DSA solution in a fixed scattering environment. As we mentioned earlier, the particle scattering can be enhanced by unstable magnetic perturbations. However, in most DSA schemes, this enhancement does not change the slope of the spectrum. It decreases the acceleration time. The scattering perturbations may saturate at a fixed $\delta B \sim B_0$ level if the particle intensity is sufficient to drive them to this level. Assuming also that the scattering supports particle diffusion with a particle diffusivity $\kappa(\epsilon, z)$, we first examine which κ might make the spectrum flat at some distance upstream, provided that the spectrum is ϵ^{-1} at and behind the shock, as observed.

Upstream particles conserve their energy as long as the second-order Fermi acceleration and the shock modification by accelerated particles are negligible. The basic DSA solution arises from a balance between convective and diffusive particle fluxes. No particle losses are assumed; particles do not escape from those parts of the shock precursor where the balance is maintained. In the shock reference frame, moving at a speed u, on its upstream ($z < 0$) side, this balance can be written down as follows:

$$\kappa(\epsilon, z)\frac{\partial F}{\partial z} - uF = 0, \tag{1}$$

where κ is the particle diffusivity in the diffusive flux from the shock, written in the form of Fick's law, and u is the flow (shock) velocity that convectively transports particles back to the shock. Note that the above equation can also be obtained by integrating Equation (8), which we will discuss later, assuming no particle injection or losses inside of the shock precursor.

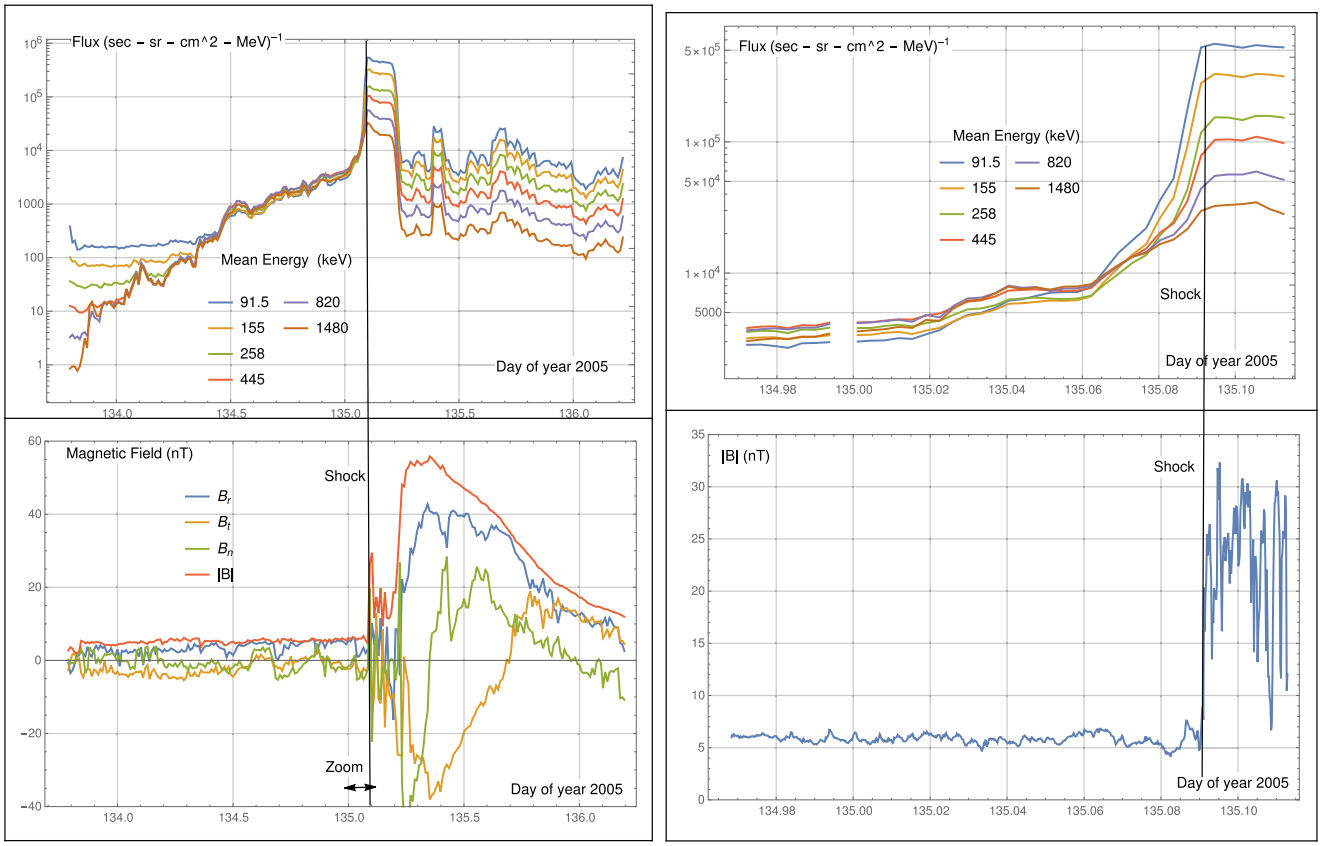

Figure 1. Top panels: EPAM 5 minute averaged solar particle fluxes. Bottom panels: MAG 16 s averaged interplanetary magnetic field data. The right two panels zoom in to a near-shock region, indicated in the bottom left panel. The data were downloaded from the ACE Science Center: http://www.srl.caltech.edu/ACE/ASC/level2.

To compare the DSA solution with the data, we use here the particle flux, $F(\epsilon)d\epsilon = f(p)vp^2dp$, with energy normalization, instead of the particle distribution, f, normalized to $4\pi p^2 dp$. Here $v = p/m$ is the particle velocity. According to the DSA, particles injected at $\epsilon \sim mu^2$ at the shock front develop the spectrum $F = Q_0\epsilon^{-s}$ for $\epsilon \gg mu^2$, where Q_0 is the intensity of seed particles extracted from the thermal pool at the shock interface. Here the index $s = (r+2)/2(r-1) = q/2 - 1$, and r is the shock compression. The derivation of s can be inferred from Equations (13) and (14). The transition of $F(\epsilon)$ between the thermal downstream core and the power-law part of the spectrum, $\propto\epsilon^{-s}$, can also be calculated analytically, given the seed extraction mechanism at $\epsilon \sim mu^2$ (see Malkov & Drury 2001 and references therein). In what follows, we focus on sufficiently high energies where the power-law dependence is established.

The data shown in Figure 1 indicate that $s \approx 1$, as predicted by the DSA for strong shocks. If s deviates from the value shown above, the balance in Equation (1) is likely to be violated (see, e.g., Section 4 below). This equation also implies that the upstream plasma, inflowing into the shock at the speed u, carries no preaccelerated particles from $z = -\infty$ ($F \to 0$), and Equation (1) remains valid up to $z = -\infty$. Not being fully consistent with the data, this assumption is not essential as long as κ does not depend on F, while both F and $\partial F/\partial z$ are negligible far upstream.

Far upstream, the flux in Figure 1 flattens abruptly in z in each energy channel, proceeding from lower to higher energy. It almost certainly manifests a preexisting background spectrum. Since it is much lower than the flux in the area of the disagreement with the DSA, we have neglected it in Equation (1) but will use it as a boundary condition when fitting the data in Section 5. Assuming here that all the accelerated particles are initially injected at the shock front from the plasma thermal core, a complete solution at $\epsilon \gg mu^2$, upstream and downstream, can be written as

$$F = \begin{cases} Q_0\epsilon^{-s}\exp\left[-u\int_z^0 \dfrac{dz}{\kappa(\epsilon, z)}\right], & z < 0, \\ Q_0\epsilon^{-s}, & z \geqslant 0. \end{cases} \tag{2}$$

Immediately behind the shock, the observed spectrum remains nearly constant (see zoom in Figure 1), which justifies the above solution at $z \geqslant 0$. However, the spectrum gradually decays at larger z. This decay contrasts evolving curved shocks with stationary plane ones, which is seen from an analytically solvable case of the DSA at expanding spherical shocks (Malkov & Aharonian 2019). Further downstream (at $t \approx 135.2$), the flux drops sharply, presumably because it crosses a magnetic "piston." It is associated with a coronal mass ejection that likely drives the shock. We will not further discuss these two downstream flux decreases, as they are unlikely to affect the upstream flattening.

Now, we test if the spectrum can be flat in an extended region upstream for any realistic κ in Equation (2). If κ grows with the particle energy and is z-independent, the energy spectrum has an isolated maximum at some $\epsilon_{\max}(z)$. It can be obtained from the equation $\kappa^2(\epsilon)/\epsilon\kappa'(\epsilon) = u|z|/s$. The spectrum is, therefore, not flat in any extended area upstream. Note that the observed particle flux decreases in the flat-

spectrum area by up to 3 orders of magnitude (depending on the energy). Therefore, we can safely reject the above scenario, in which κ is z-independent everywhere upstream.

Based on the upper right panel of Figure 1, the spectrum flattens at $z < z_0$, where z_0 roughly corresponds to $t = 135.06$. If the solution in Equation (2) applies, F must be energy-independent at $z = z_0$, but it still must decrease as ϵ^{-s} at $z = 0$. From Equation (2), we thus have

$$u \int_{z_0}^{0} \frac{dz}{\kappa(\epsilon, z)} = s \ln \frac{\epsilon_0}{\epsilon}, \tag{3}$$

where $\epsilon_0 > \epsilon$ relates to the normalization of F. Beyond z_0, the spectrum is observed to be flat. We can infer the transition point z_0 from the observations, which is about the same for all energy channels. The above relation means that the quantity $\overline{\kappa^{-1}}$ (z-averaged over $z_0 < z < 0$) must decrease with energy as $\ln(\epsilon_0/\epsilon)$. This relation does not, however, fully constrain the turbulence spectrum in the area $z_0 < z < 0$. We will return to that constraint later.

The spectral flatness at $z < z_0$ requires κ to be ϵ-independent in this area. To examine whether physically reasonable wave spectra can meet this requirement and Equation (3), let us start with the most straightforward possibility, assuming that the particle diffusion is field-aligned. It is a good approximation if the wave amplitudes are moderate and the angle between the shock normal and magnetic field, $\vartheta_{\rm Bn}$, is not too close to $\pi/2$: $\delta B^2/B_0^2 < \cot\vartheta_{\rm Bn}$ (Section 3). A common DSA assumption is that the particle cyclotron resonance with waves supports their diffusion, so $k_\parallel \approx \omega_c/v_\parallel$, where $v_\parallel$ is the particle velocity along the field. It is assumed that the wave frequency $\omega \ll \omega_c$. Hence, for the diffusion coefficient, we have $\kappa \sim \kappa_\parallel \propto v^3/\delta B_k^2$ (e.g., Lee 1982). This relation links z with ϵ by virtue of Equation (3) because δB_k depends on z. Namely, it requires a z-averaged magnetic fluctuation spectrum to be $\delta B_k^2 \propto k^{-3}\ln(k/k_0)$ within $z_0 < z < 0$, where $k_0 = \omega_c/\sqrt{2\epsilon_0/m}$. Since $\kappa \propto v^3/\delta B_k^2$, it becomes energy-independent if we neglect the logarithmic dependence on k of $\overline{\delta B_k^2}$ or assume that the z-averaging somehow compensates for this insignificant factor, compared to k^{-3}, in the spectral density. These are relatively mild changes, though. For $z < z_0$, one thus obtains $\delta B_k^2 \propto k^{-3}$, which makes κ roughly energy-independent, as required for the flat spectrum. Let us now consider the possibility of generating the k^{-3} spectrum.

2.2. Constraining the Underlying Wave Turbulence

The turbulence spectrum often discussed as being resonantly generated by accelerated particles is the k^{-2} spectrum, associated with nonrelativistic particles (Lee 1983; Forman & Webb 1985), and k^{-1}, associated with the relativistic ones (Bell 1978). Both cases are valid for the $r = 4$ shock compression ratio, thus corresponding to the p^{-4} spectrum downstream (normalized to p^2dp). Resonant wave–particle interactions without wave cascading are employed in obtaining these results. The steep k^{-3} wave spectrum, inferred in the preceding subsection, would correspond to a very flat, p^{-3} particle spectrum at and behind the shock. The latter is hardly possible, as even in the limit of much more powerful shocks, strongly modified by particles accelerated to ultrarelativistic energies, the flattest asymptotic downstream spectrum is $p^{-3.5}$ (Malkov & Drury 2001). However, the spectrum in question, corresponding to $F(\epsilon) = \text{const}$, is observed farther upstream. As we mentioned, Lee's theory relates the wave spectrum upstream to the particle spectrum downstream, which is an oversimplification in describing the flat upstream spectra.

According to Figure 1, the spectrum remains flat despite decaying by 2–3 orders of magnitude upstream. This behavior is counterintuitive and defies the standard DSA principles. Indeed, particles observed far upstream have likely spent most of their last acceleration cycle (crossing and recrossing the shock, gaining $\sim U_{\rm sh}/v$ of their current energy) while balancing between the convection with the flow toward the shock and diffusing against it. Diffusion generally intensifies with the particle energy, which should lead higher-energy particles to diffuse farther upstream. It seems they should break the spectrum flatness, whatever mechanism maintains it up to a certain distance. On the contrary, the spectrum remains flat in a wide area upstream.

Unstable waves, initiated far upstream, where the particle flux is low, are convected with the flow to the shock, and their growth rate must increase along with the particle flux. The turbulence intensifies if no significant instability suppression (quasi-linear or nonlinear) occurs. Eventually, it may saturate and change its spectral shape before a fluid element crosses the shock. The question is why and how the particle spectrum remains flat, whereas the transport driving turbulence evolves. To answer this question, we consider the following scenario.

When the wave and particle flux grow toward the shock, the particle transport goes nonlinear, thus making their diffusivity, κ, flux-dependent (Bell 1978; Lee 1982). Meanwhile, the resonant wave–particle interaction, which is behind the quasi-linear calculations of particle transport in the above references and Section 2.1, ceases to apply if the wave amplitudes grow beyond the level of a resonant, quasi-linear regime of the wave–particle interaction. Assuming further that the waves are nonresonantly driven by a pressure gradient of energetic particles (Drury & Falle 1986), we may use some results of Malkov & Moskalenko (2021). According to them, an ensemble of weak shocks (shocklets) generated by the pressure gradient evolves toward longer scales by shock mergers (inverse turbulence cascade). As their strength increases, the spectrum develops a magnetic turbulence component transferring to shorter scales (forward cascade). The magnetic part of the turbulence supports particle scattering, thus controlling their spatial transport. The forward cascade flattens the spectrum to a $k^{-3/2}$ Iroshnikov–Kraichnan (IK) spectrum (Iroshnikov 1964; Kraichnan 1965).

The IK spectrum is not a prerequisite for flat particle flux, as shown in the sequel. Nonetheless, Perri et al. (2023) have identified the wave spectrum $k^{-1.51}$ precisely in the area of the flat particle spectrum (see Figure 4 in their paper). Compared to the canonical DSA spectrum (k^{-2} in a nonrelativistic regime), the IK spectrum contains more energy in shorter scales. Given their significant amplitudes, a particle suffers many scattering events while interacting with a broad range of waves, still much shorter than its Larmor radius. In effect, it accumulates a significant deflection before completing its Larmor rotation.

By contrast, most of the DSA studies rely on resonant wave–particle interactions, assuming a low-amplitude, random-phase wave spectrum with $\delta B_k \ll B_0$. In some cases, though not frequently, an opposite approximation of a single dominant wave with $\delta B_1 \gtrsim B_0$ in a broad quasi-linear $\delta B_k \ll B_0$ continuum compares positively with simulations and even

observations (see, e.g., Hanusch et al. 2019 and references therein). These approaches do not work for the case at hand, both de facto and because the required conditions do not hold. As seen from Figure 1, separate field components reach the level $\delta B \gtrsim B_0$ and often form coherent short-scale structures. If the spectrum is sufficiently flat and intense, particles with a large Larmor radius should be deflected by such perturbations multiple times during each rotation. For sufficiently large amplitudes, an approximation based on a sequence of uncorrelated particle deflections by the magnetic perturbations with the scales $l \ll r_g$ but large-amplitude $\delta B_l \gtrsim B_0$ has proved more accurate.

As the IK spectrum is significantly flatter than Lee's resonant k^{-2} spectrum, we may assume that the wave–particle interaction with high-energy particles is dominated by a $kr_g \gg 1$ condition that is essentially nonresonant. At the same time, the phases of the short-scale magnetic perturbations are randomized as the waves cascade to shorter scales. The nonresonant transport is then easily calculated in the above-described, well-known fashion. One starts with an angular diffusion in momentum space, assuming that by crossing the turbulence correlation length, l, particles deflect only by a small angle $\delta\vartheta$. For the angular diffusion rate, we find $\nu = \Delta\vartheta^2/2t \sim (lv/r_g^2)(\delta B_l/B_0)^2$. Here, we assumed that the angle $\Delta\vartheta$ is accumulated from $vt/l \gg 1$ uncorrelated deflections, each of which is at an angle $\delta\vartheta \sim (l/r_g)(\delta B_l/B_0)$. Note that unlike the standard quasi-linear derivation that we applied to the resonant wave–particle interaction leading to the parallel diffusion $\kappa_\parallel \propto v^3/\delta B_k^2$, the length scale l in the amplitude δB_l is not related to the particle velocity, v. Thus, by defining the parallel diffusion in a standard way as $\kappa_\parallel = v\lambda/3$ with the particle mean free path, $\lambda = v/\nu$, we arrive at the following expression for $\kappa_\parallel$:

$$\kappa_\parallel = \frac{v^2}{3\nu} \sim \frac{v^3}{l\omega_c^2}\left(\frac{B_0}{\delta B_l}\right)^2. \tag{4}$$

Since l is a fixed turbulence correlation length, it is not associated with the resonant wavenumber $k = r_g^{-1} \propto 1/\sqrt{\epsilon}$; the parallel diffusivity scales with energy as $\kappa_\parallel \propto \epsilon^{3/2}$, instead of $\kappa_\parallel \propto \epsilon^{3/4}$, which one would obtain in the case of a resonant particle diffusion, specifically for the IK spectrum.

3. Possible Regimes of Particle Self-confinement

To fit the data shown in Figure 1, in this section, we introduce some further modifications to the "standard" DSA mechanism. We also justify simplifications, such as a planar and stationary shock assumption, that we will use later. Although the diffusion–convection balance essentially controls particle transport upstream, similarly to Equation (1), we now also allow for an injection of thermal particles at the shock discontinuity and an escape of accelerated and influx of preexisting energetic particles from the far-upstream space. Therefore, the total particle flux, diffusive plus convective, across the shock precursor is not exactly zero, although it is much smaller than its primary components.

Freshly injected particles are vital for spectral flatness. Indeed, some 4 orders of magnitude of enhancement of the particle flux at the shock, compared to the background ($z = -\infty$), would be impossible by a mere reacceleration of the background population, preexisting far upstream. The reaccelerated flux enhancement would hardly exceed a factor of a few, depending on the shock compression and the background upstream spectrum. This aspect of the DSA was discussed in detail by Malkov & Moskalenko (2021) in conjunction with a recently discovered fine structure in a galactic cosmic-ray spectrum, which is also deemed incompatible with the "standard" DSA, assuming that the DSA is responsible for the cosmic-ray acceleration.

On the far-upstream end of the flat-spectrum region, the simple diffusion–convection balance in Equation (1) needs to be supplemented with the background cosmic rays convected into the shock precursor and the shock-accelerated cosmic rays diffusively leaked from it. Inside the flat-spectrum region and in the shock vicinity, the particle flux is greatly enhanced over the background level, which couples it with the wave intensity. By contrast, a simple relation between the particle flux and wave intensity is not accurate in the far-upstream region, where both quantities approach their background levels and decouple. Their intensities are generally unrelated to each other. Therefore, a linear relation between the particle flux and wave energy density introduced below by Equation (7) contains a model parameter, ψ. It is, however, essential only in the transition region to the background energetic particles and does not significantly affect most of the shock precursor where the flat particle flux is observed.

The spatial downstream distribution of shock-accelerated particles is qualitatively sensitive to even a gradual time dependence of the shock speed and its front curvature. In a steady planar shock, the downstream distribution is homogeneous. If the shock slows down and expands in a self-similar way, e.g., after a point explosion, the distribution of accelerated particles is more complicated but can still be obtained from a self-similar solution (Malkov & Aharonian 2019). The solution shows that the particle distribution decays behind the shock as well. This self-similar solution is relevant to the downstream particle distribution shown in Figure 1 because coronal mass ejection shocks in the heliosphere are also curved and decelerating. However, the gradual flux decrease shown in Figure 1 and interpreted in the above sense is not critical for the upstream flattening. Hence, the stationary and planar shock approximation with a constant flux downstream in studying the upstream flattening appears justified.

The shock under consideration has been found to be oblique with $\vartheta_{\rm Bn} \approx 62^\circ$ (Perri et al. 2023). So, we also need to estimate the effect of transport anisotropy. It is characterized by two components of the diffusion tensor, $\kappa_\parallel$ and $\kappa_\perp$, along and across the magnetic field, respectively. Their combination governs the diffusion along the shock normal, $\kappa = \kappa_\parallel \cos^2\vartheta_{\rm Bn} + \kappa_\perp \sin^2\vartheta_{\rm Bn}$. Since the value $\tan^2(\vartheta_{\rm Bn}) \approx 3.5$ is relatively large, $\kappa_\perp$ may significantly contribute to the particle diffusion immediately ahead of the shock, where it is enhanced, and $\kappa_\parallel$ is suppressed by a self-driven turbulence. However, $\kappa_\perp \ll \kappa_\parallel$ where the magnetic field fluctuations remain limited to $\delta B \lesssim B_0$, as we discussed at the end of Section 2.1. Therefore, $\kappa_\perp \sim \kappa_\parallel$ only in a narrow region ahead of the shock. Farther upstream, where the spectrum flattens, the cross-field diffusion decreases, as the wave energy $E_{\rm w}$ does, while $\kappa_\perp \sim \kappa_\parallel E_{\rm w}^2$ (the dimensionless wave energy $E_{\rm w}$, normalized to the background magnetic field energy, is introduced below). A rough estimate of $E_{\rm w}$ in the upstream area adjacent to the shock can be made by assuming that the wave pondermotive pressure exerted on particles is equilibrated by their partial pressure (see Equation (7) below). It shows that $E_{\rm w} \sim$

$\sqrt{\epsilon/m}\,\epsilon F(\epsilon)/n_0 V_A^2$. Here $n_0 = \rho/m$ is the plasma density. By scaling E_w down from its maximum value at $\sqrt{\epsilon/m} \sim 10^9$ cm s^{-1}, assuming $n_0 \sim 1$ cm^{-3}, $V_A \sim 10^7$ cm s^{-1}, we can place the following upper limit: $E_w \lesssim 10^{-5}\epsilon F(\epsilon, z)$. By noting that $\epsilon F(\epsilon, z = 0) \approx$ const $\approx 5 \times 10^5$ (Figure 1), while sharply decreasing at $z < 0$, we conclude that the quasi-linear treatment of the wave interactions with plasma we invoke below in the flat region is tenable.

In the flat-spectrum region, the ϑ_{Bn} appears to decrease compared to the near upstream, though with considerable variations. These trends can be gleaned from Figure 1 in Perri et al. (2023). Therefore, $\kappa_\perp$ might significantly contribute to the particle diffusion upstream only in a relatively narrow transition zone between the shock and the flat-spectrum area, where E_w attains its maximum at $E_w \sim 5$. In this transition zone, low-energy particles exhibit a steeper flux decay, which is necessary to converge to the flat particle flux farther upstream. In understanding the nature of this spatial decay, one needs to consider the angular particle dynamics in momentum space underlying the diffusive approximation. As we see from Figure 1 (bottom right), the $|B|$ profile makes traps and magnetic barriers for the particles immediately ahead of the shock. It is reasonable to assume that the trap adjacent to the shock is filled with the downstream ϵ^{-1} particles, leaking in the upstream direction and forming the flat spectrum. We can conjecture that these magnetic structures regulate the particle leakage, making their flux almost energy-independent, at least in this particular case of the 2005 May shock.

Consider such a magnetic trap near the shock front. Its loss-cone angle is defined by the trap's mirror ratio, B_{min}/B_{max}, so that only particles that have pitch angles at the bottom of the trap $\sin^2\alpha < B_{min}/B_{max}$ may leak through the trap's barrier where B approaches B_{max}. Adiabaticity of particle motion is assumed but increasingly violated for higher energies, so these particles are more likely to leak, thus facilitating the formation of energy-independent flux upstream. The energy-biased leakage mechanism warrants a separate study, which is beyond the scope of this paper. An observationally learned fact is that the leaking particle flux becomes and remains flat farther upstream of the trap. The flat flux sustainability is the focal point of this study.

On a practical note, neglecting $\kappa_\perp$ allows us to solve Equation (9) below in explicit form. With $\kappa_\perp$ included, it can be solved implicitly via an inverse function $z(F, p)$, which would only obscure the interpretation of the result but give us no further insight into the physics of the spectral flattening. As we will see, the parallel diffusion alone supports a rapid transition of the power-law spectrum at the shock, which is close to ϵ^{-1}, into the flat spectrum upstream. Therefore, neglecting the cross-field diffusion in a narrow layer adjacent to the shock, where E_w approaches unity and possibly even exceeds it, appears commensurate with this level of consideration.

For the field-aligned diffusion, we follow Bell's approach to its quasi-linear suppression by Alfvén waves generated by accelerated particles upstream (Bell 1978), except the wave–particle interaction is nonresonant in our case. We define the dimensionless wave spectral density, E_w, already used above, by relating it to the rms magnetic field fluctuations, $\langle \delta B^2 \rangle$, and the background field, B_0, as follows:

$$\frac{\langle \delta B^2 \rangle}{B_0^2} = \int E_w(k) d\ln k = \int E_w(p) d\ln p.$$

The last relation conveniently implies an inverse dependence $p \propto k^{-1}$ (Skilling 1975), although we do not impose the resonance relation $\rho_g(p)k \sim 1$. Note that we use the same notation E_w for the p- and k-dependent spectral densities, which should not lead to confusion. We also use the physical arguments of Blandford (1980) and Drury (1983) about the relation between the wave generation and the work done by the pressure of accelerated particles on the fluid. For that purpose, we introduce a dimensionless partial pressure of energetic particles and normalize it, as E_w, to $d\ln p$:

$$P(p) = \frac{8\pi}{3\rho V_A^2} v p^4 f, \tag{5}$$

where f is the ordinary particle distribution function normalized to $4\pi p^2 dp$. The wave-generation rate upstream of the shock can be obtained from the rate at which the pressure of energetic particles does work on the waves. The waves are propagating oppositely to the inflowing plasma, so their speed in the shock frame is $u - V_w$, with $V_w \approx V_A$. Balancing the wave ponder-motive pressure with that of the energetic particles (e.g., Drury 1983), we have (see also the Appendix)

$$(M_A - 1)\frac{\partial E_w}{\partial z} = \frac{\partial P}{\partial z}, \tag{6}$$

where $M_A = u/V_A$ is the shock Alfvén Mach number. This equation extends the pressure balance principle to a detailed balance that, generally speaking, requires the wave–particle resonance that we do not assume. However, the balance is crucial for the coordinate dependence of P and E_w, not on momentum and wavenumber. For a successful fit of the particle spectrum in the entire upstream region, it is also essential that E_w and P decouple far from the shock front, where they approach the respective background levels. Thus, after integration, we ought to write

$$E_w = \frac{16\pi\sqrt{2m}\,\epsilon^{3/2}}{3(M_A - 1)\rho V_A^2}(F + \psi). \tag{7}$$

Here $\psi(p)$ is an arbitrary function of particle momentum mentioned earlier and $F(\epsilon, z)d\epsilon = vp^2 f(p)dp$ is the particle flux normalized to $Fd\epsilon$, as introduced in Equation (1). We will use this quantity instead of f and P for fitting the solution to the data. It might appear plausible to obtain ψ from the far-upstream values of E_w and F, i.e., at $z = -\infty$. However, the underlying Equation (6) is valid in a strongly nonlinear particle transport regime in which both particle and wave intensities are high; other terms become essential when the particle pressure gradient decreases to the background level. Additional wave processes other than their convection and generation by the particle pressure in Equation (6) need to be included, such as linear damping, wave steepening, and nonlinear Landau damping. Thus, $\psi(p)$ remains undetermined at this level of the model. However, as we will see, ψ does not affect the fit in most of the shock precursor and is essential only at the

transition to the spatially independent background particle flux far upstream.

4. Acceleration Model

We now return to Equation (4) and rewrite it as follows: $\kappa_\parallel = \kappa_0/E_w$, with $\kappa_0 \propto \epsilon^{3/2}$. To make contact with traditional treatments, at first we use the distribution function with the particle density normalized to fp^2dp and will return to the particle flux $F(\epsilon)$ for a comparison with the data later. The stationary convection–diffusion equation for f at the shock front has the following form:

$$u\frac{\partial f}{\partial z} = \frac{\partial}{\partial z}\kappa_\parallel \cos^2\vartheta_{\rm Bn}\frac{\partial f}{\partial z} - \frac{p}{3}\Delta u\frac{\partial f}{\partial p}\delta(z) + Q(p)\delta(z). \quad (8)$$

The last two terms on the right-hand side are associated with the particle acceleration on the velocity jump $\Delta u \equiv u - u_{\rm d}$, preceded by their injection at the rate Q from a thermal plasma core (Malkov & Drury 2001). Here u is the upstream flow speed, as before, and u_d is the downstream flow speed, both measured in the shock frame.

Let us integrate Equation (8) within the upstream region ($z < 0$, two last terms on the right-hand side dropped):

$$E_w^{-1}\cos^2\vartheta_{\rm Bn}\kappa_0\frac{\partial f}{\partial z} - uf(z) = \Phi(p). \quad (9)$$

We have introduced κ_0 here by $\kappa_0 = \kappa_\parallel E_w$, which we will fully specify in Section 5. The integration constant $\Phi(p)$ is thus minus the total z-independent particle flux (diffusive plus convective) on the left-hand side. If Φ is known, we can determine the particle distribution at the shock, $f_0(p)$, which is observed to decay approximately as p^{-4}, as in strong shocks. The particle distribution $f(p, z)$ flattens upstream to p^{-2}. Based on the observations shown in Figure 1, the flattening occurs over a short distance where the particle intensity declines progressively more steeply in the upstream direction as the particle energy decreases. In the traditional DSA framework, $\Phi(p)$ can be specified using the far-upstream convective flux $\Phi = \Phi_\infty = -uf(-\infty, p) \equiv -uf_\infty(p)$, provided that $\partial f/\partial z \to 0$, $E_{\rm w} \neq 0$ at $z \to -\infty$. However, given the data shown in Figure 1, there are problems with this identification of $\Phi(p)$, which we discuss below.

A decaying particle flux upstream in Figure 1 abruptly changes to a constant $f_\infty(p)$ in all energy channels at $z = -z_\infty(p)$. The value of z_∞ is larger, and the transition is sharper at higher particle energies. With good accuracy, the derivative $\partial f/\partial z$ can be regarded as discontinuous at $z = -z_\infty$. Hence, in the context of the convection–diffusion problem formulated in $z \in (-\infty, \infty)$, the break at $z = -z_\infty$ in the particle spectrum (a jump of $\partial f/\partial z$) requires an extra term $-S(p)\delta(z + z_\infty)$ on the right-hand side of Equation (8). It effectively represents a particle sink, similar to the source of injected particles $+Q\delta(z)$ but with an opposite sign. Physically, it means that upon diffusing to the point $z = -z_\infty$ against the plasma flow, particles injected and accelerated at the shock front earlier promptly escape toward $-\infty$.

It is worthwhile to compare the boundary z_∞ with a so-called free-escape boundary (FEB), broadly used in Monte Carlo simulations of the DSA (e.g., Ellison et al. 1990). There is a significant physical difference between the z_∞ and FEB. Namely, z_∞ depends strongly on p, while the FEB in simulations typically does not. Another practical observation is that $z_\infty(p)$ is primarily defined by the background spectrum $f_\infty(p)$, at least for the flat particle fluxes shown.

Since the particle distribution is constant outside of the interval $(-z_\infty, 0)$, it is plausible to formulate the boundary value problem for Equation (8) in the finite interval $z \in (-z_\infty, 0)$ upstream instead of $z \in (-\infty, 0)$, which would be typical for the traditional DSA. We therefore must set $f = f_\infty(p)$ as the left boundary condition at $z = -z_\infty$. Both f_∞ and z_∞ can be extracted from the data in all energy channels to calibrate the acceleration model in the next section.

As a second boundary condition for Equation (8), it is natural to set $f = f_0(p)$ at $z = 0$. We will argue that it is also worth extracting from the data rather than calculating it using shock parameters. The difference with the left boundary condition is that f_0 can, ideally, be obtained "from the first principles" by integrating Equation (8) across $z = 0$, which yields the following differential equation for f_0:

$$\Phi(p) = -uf_0 - \frac{p}{3}\Delta u\frac{\partial f_0}{\partial p} + Q(p) \equiv \Phi_0, \quad (10)$$

where $\Phi(p)$ is the same integration constant in Equation (9). It is instructive to return for a moment to the traditional DSA, in which one sets $\Phi_0 = \Phi_\infty = -uf_\infty(p)$. By substituting this relation into Equation (10), one then obtains the solution $f_0(p)$ at and behind the shock. However, this approach to obtaining the integration constant $\Phi(p)$ in Equation (9) has the following problems.

First, the accuracy of Equations (8) and (9) is questionable near the shock, since the quasi-linear expression for the diffusive flux is not a good approximation where the wave intensity is high, and the particle intensity changes sharply. Second, the shock speed parameters u and $u_{\rm d} \equiv u - \Delta u$ entering Equation (10) significantly fluctuate near the shock transition. For example, Perri et al. (2023) indicate a strong deviation for the shock compression, $r \equiv u/u_{\rm d} = 3.0 \pm 0.6$. So, this parameter does not define the spectrum accurately. Third, we have neglected the cross-field transport, which will likely be significant near the discontinuity. Lastly, available analytic calculations of the injection rate $Q(p)$, which are needed for computing $f_0(p)$ in Equation (10), still require a seed particle source at $p \sim mu$ (Malkov & Drury 2001). The simulations are generally helpful, but they still have significant disagreements. They become particularly evident when comparing particle injection into the DSA with different mass-to-charge ratios (A/Q; see Hanusch et al. 2019 and references therein). Hanusch et al. (2019) scrutinizes numerical and analytical injection models using their predictions of A/Q injection patterns of different ions. Indeed, trajectories of nonrelativistic particles in electromagnetic fields are differentiated by this ratio, as opposed to the ultrarelativistic particles for which the rigidity defines the trajectory.

In light of these problems, we extract $f_0(p)$ for a boundary condition in Equation (9) at $z = 0$ directly from the data. It provides a more stable time-averaged boundary value than we could possibly calculate using Equation (10), given the uncertainties listed above. Within this formulation, we will at first regard the total particle flux across the shock precursor, Φ, as a free parameter that will be determined from the boundary condition at $z = -z_\infty$, at which it transitions into the particle flux escaping the shock to $z = -\infty$.

5. Solving and Calibrating the Acceleration Model

After expressing the wave energy density $E_w(z, \epsilon)$ in Equation (9) and the particle distribution f through the particle flux F using Equation (7) and the relation $F(\epsilon)d\epsilon = f(p)vp^2dp$, respectively, we evaluate Equation (9) to the following form:

$$K(z)\frac{\kappa_0(\epsilon)\epsilon^{-3/2}}{F+\psi(\epsilon)}\frac{\partial F}{\partial z} - F = \Psi(\epsilon), \tag{11}$$

where we have introduced the notation

$$K \equiv \frac{3\rho V_A(1-M_A^{-1})}{16\pi\sqrt{2m}}\cos^2\vartheta_{Bn}(z); \quad \Psi(\epsilon) = \frac{2m}{u}\epsilon\Phi. \tag{12}$$

Recall that ψ and Ψ emerged from the integration of the wave production balance in Equation (6) and that of the convective–diffusive particle transport in Equation (8), respectively. As we discussed in the previous section, Ψ can be formally expressed through the particle injection rate Q and the upstream and downstream flow speeds u and u_d, using Equation (10). By omitting Q for nonthermal particles, for Ψ, we have

$$\Psi(\epsilon) = -\frac{\epsilon^{-s+1}}{s+1}\frac{\partial}{\partial\epsilon}\epsilon^s F_0. \tag{13}$$

Here, we have converted the power-law index q, introduced earlier for $f_0(p)$, to its equivalent for $F_0 = F(\epsilon, z = 0)$:

$$s = \frac{3u}{2\Delta u} - 1 = \frac{q}{2} - 1. \tag{14}$$

Although the contribution of the injection term Q is negligible at high energies, it defines the normalization of F_0 and thus Ψ. However, $\Psi(\epsilon)$ vanishes where F_0 follows the DSA spectrum $\propto\epsilon^{-s}$, but as s is known only approximately, we keep Ψ in the analysis. The opposite is also true: if $\Phi_0 = Q = 0$ in Equation (10), and thus $\Psi = 0$, the spectrum F_0 obeys the standard DSA power law with the index s given above. Since we use a steady-state model, while the shock parameters likely fluctuate, it is difficult to calculate Ψ a priori. A more plausible approach is to extract it by fitting the solution of Equation (11) to the data, although we will constrain Ψ below.

The measured downstream spectrum closely follows the DSA predictions if one takes the uncertain compression ratio close to or slightly above the upper bound given by Perri et al. (2023), $r = 3.6$. It means that Ψ is small compared to F_0 and even $F(z)$ in a significant part of the shock precursor, $\Psi \ll F$. Other than that, Ψ is largely unconstrained, as long as we do not specify the injection efficiency and shock compression. To minimize the number of parameters it depends upon, we will represent Ψ by a power-law function of ϵ with an amplitude and index extracted from the data rather than precalculated from the relation in Equation (13).

Turning to the parameter ψ, from Figure 1, we see that near $z = -z_\infty$, F is way below its values almost across the entire shock precursor. By Equation (6), the same conclusion can be drawn for E_w. Hence, $\psi(p)$ in Equation (7) must also be small compared to F, except near $z = -z_\infty$. Summarizing the above considerations, we treat Ψ and ψ as free parameters and use F_0 and F_∞ as more reliable inputs for the model since we determine them directly from the data. However, we have also used them to constrain the less certain parameters Ψ and ψ.

After introducing a normalized distance ζ in place of z, which has the dimensionality of $1/F$,

$$\zeta = \frac{\epsilon^{3/2}}{\kappa_0(\epsilon)}\int_0^z \frac{dz'}{K(z')}, \tag{15}$$

Equation (11) rewrites as

$$\frac{1}{F+\psi}\frac{\partial F}{\partial\zeta} - F = \Psi. \tag{16}$$

The flat spectrum requires the following two conditions: ζ is ϵ-independent and $F \gg \psi(\epsilon)$. We obtain a solution that also satisfies the boundary condition $F(0, \epsilon) = F_0(\epsilon)$ for arbitrary values of parameters ψ and Ψ:

$$F = (\Psi - \psi)\left[\left(1 + \frac{\Psi-\psi}{F_0+\psi}\right)e^{(\psi-\Psi)\zeta} - 1\right]^{-1} - \psi. \tag{17}$$

The solution at large negative ζ, which we associate with an area of far-upstream transition to the background population of energetic particles, depends on Ψ and ψ. Remarkably, in the near-upstream area of transition from the downstream spectrum $F_0(\epsilon)$ to the broad flat-flux area, including the latter, the solution is insensitive to these parameters. It is, therefore, worthwhile to begin the solution analysis with small negative ζ since it helps understand how this transition from the downstream $F_0(\epsilon)$ to the flat upstream distribution occurs.

5.1. Near- and Mid-upstream Zones

By developing the general solution F in Equation (17) in a Taylor series in $|(\psi - \Psi)\zeta| \ll 1$ and assuming, as argued earlier, that $\psi \ll F$ in most of the shock precursor, we find that within these approximations, F does not depend on Ψ or ψ:

$$F \simeq \frac{F_0}{1 - F_0\zeta}. \tag{18}$$

Using the data, we fit $F_0(\varepsilon)$ by $F_0 \propto \epsilon^{-\sigma}$, where $\sigma \approx 1.03$ (Table 1). In order to compare this result with the data shown in Figure 1, we need to convert the normalized distance to the shock, ζ, to the spacecraft time used in that figure. We first relate the time to the physical distance as follows: $z = U_{sc}(t - t_{sh})$, where U_{sc} denotes the spacecraft speed relative to its shock-crossing point at the time instance t_{sh}. This conversion may contain some geometrical uncertainty associated with a possibly oblique motion of the shock front relative to the spacecraft. However, it combines with an uncertainty in κ_0 parameterization in Equation (15). Using Equation (4), it is convenient to represent κ_0, introduced earlier as $\kappa_0 = \kappa_\parallel E_w$, as follows:

$$\kappa_0 \approx \left(\frac{\epsilon}{\epsilon_1}\right)^{3/2}\frac{v_1^2}{\omega_{ci}}w, \quad \text{where } w \sim \frac{v_1}{l\omega_{ci}},$$

and where $\epsilon_1 = 91.5$ keV is the particle energy in the lowest energy channel that we use in our analysis, $v_1 \approx 3\times10^8$ cm s^{-1} is the respective particle velocity, and l is the dominant scale of nonresonant magnetic perturbations responsible for particle scattering. Here, w is a free parameter of the model, which is of the order of the ratio of the Larmor radius of the particles with velocity v_1 to the turbulence scale l. The advantage of

Table 1
Input Functions and Parameters for Equation (17)

	Function of ϵ(keV)				Parameters									
	F_0	Ψ	ψ	ζ	C_0	C_Ψ	C_ψ	C_ζ	σ	γ	ρ	μ	ϵ_1	$t_{\rm sh}$
Fit	$C_0(\epsilon_1/\epsilon)^\sigma$	$C_\Psi(\epsilon_1/\epsilon)^\gamma$	$C_\psi(\epsilon_1/\epsilon)^\rho$	$C_\zeta(\epsilon/\epsilon_1)^\mu(t-t_{\rm sh})$	5.5×10^5	685	185	2.61×10^{-3}	1.03	0.103	0.14	0.04	91.5 keV	135.091 (DoY)
Equation/BC	BC	Equation (13)	Equation (7)	Equation (15)										

Note. The downstream normalization constant, C_0, and the power-law index σ are extracted directly from the spectrum downstream. Other parameters are obtained by fitting the data, including the breaking points at $z=-z_\infty$, to Equation (17), shown in Figure 3 (see text).

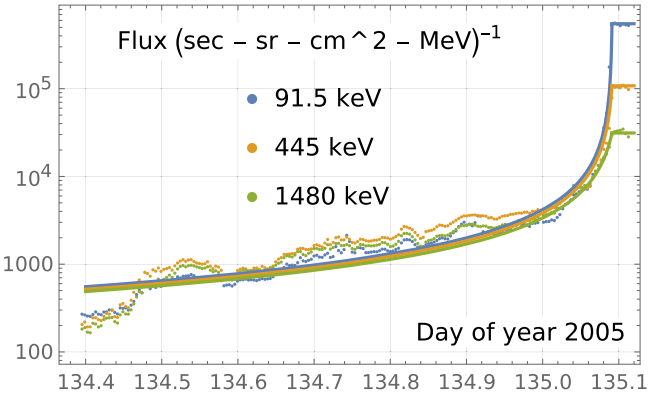

Figure 2. Approximate solution in Equation (18) shown in three energy channels indicated in the plot.

separating w from the ϵ-scaling of κ_0 is in that the uncertainty in l now combines with the abovementioned uncertainty of the shock geometry in the definition of the normalized distance ζ in Equation (15). Both of these uncertainties will be absorbed in a single fitting parameter C_ζ given in Table 1. We will discuss other aspects of the mapping $z \to \zeta$ when presenting the full fit of the solution in Equation (17) to the data shown in Figure 1 in the next subsection.

We plot the formula in Equation (18) against time and compare the result with the data in Figure 2. For clarity, we have selected three representative energies from the six shown in Figure 1. Apart from a good agreement with the data, the simplified expression in Equation (18) does not include the uncertain model parameters Ψ and ψ. This expression thus embodies the universality of the underlying flattening mechanism. The model parameters are lumped here in a single variable, ζ, defined in Equation (15). They include a combination of the wave turbulence level; its characteristic scale, l, most vital for the particle scattering; the local field angle $\vartheta_{nB}(z)$; the plasma density; the magnetic field strength; and the spacecraft trajectory angle relative to the shock surface, mentioned above. Some of these quantities are uncertain and even fluctuate, but we combine them in a single constant C_ζ in Table 1 to describe this multivariable combination. For better agreement with the data far upstream, considered below, we have also included a small correction to the $\kappa_0 \propto \epsilon^{3/2}$ scaling by representing it as $\epsilon^{3/2-\mu}$, with $\mu = 0.04$.

When comparing the model prediction with the data shown in Figure 1, we note that they provide only a single-pass scan of the particle intensity with no direct information about their possible time variability. The DSA acceleration time, however, is typically the shock-crossing time of its precursor filled with the accelerated particles, $\tau_{\rm acc} \sim \kappa/U_{\rm sh}^2$. Although this estimate is strictly applicable to a linear acceleration regime with a prescribed, flux-independent $\kappa(\epsilon)$, it can be shown to also apply to strongly nonlinear particle acceleration in shocks modified by their pressure (Malkov & Drury 2001). The case we consider belongs to neither of the above. However, the acceleration time is much longer than the shock parameter variation timescale, which can be inferred from the short-scale variation of the plasma and particle data across the precursor. As our model is stationary, the deviations of the real data from the theoretical curve are expected. The agreement may be partly improved by including the z dependence of ϑ_{nB} in the definition of ζ. However, the nonmonotonic parts of the particle intensity cannot be corrected within the steady-state model. We will return to the observed deviation in Section 7.

Since $\Psi, \psi \ll F_0$, we can further simplify the expression in Equation (18) for larger $-\zeta$ without violating its applicability condition, $|(\psi - \Psi)\zeta| \ll 1$. In this approximation, the upstream spectrum $F(\zeta)$, $\zeta < 0$ ceases to depend on ϵ *explicitly*. The transition to this regime occurs over a narrow interval adjacent to the shock, $-1/F_0 \lesssim \zeta < 0$, where the range of $1/F_0$ is roughly $2 \times 10^{-6} < 1/F_0(\epsilon) < 3 \times 10^{-5}$. To the left of this interval, i.e., for $\zeta < -1/F_0$, the spectrum depends only on ζ and can be approximated as

$$F \approx -1/\zeta \tag{19}$$

up to the far upstream, where it gradually decreases to $F \sim \psi$ or $F \sim \Psi$, whichever occurs closer to the shock. In this universal $1/\zeta$ regime, the energy dependence may only be through the normalized distance ζ, defined in Equation (15) and discussed at some length above. As we have shown, for a nonresonant particle scattering, the particle diffusivity must scale close to $\kappa_0(\epsilon) \propto \epsilon^{3/2}$ (Equation (4)). Therefore, ζ does not depend on ϵ, and the asymptotic solution $F \approx -1/\zeta$ is, indeed, perfectly flat.

Most of the spectrum is thus describable by a simple formula in Equation (18), simplifying even further beyond a narrow layer upstream of the shock surface. A salient feature of this solution is that the uncertain model parameters $\psi(\epsilon)$ and $\Psi(\epsilon)$ do not enter it. All essential aspects of this solution are encapsulated in the single variable ζ. Yet it agrees with the data, as shown in Figure 2. However, some deviations are present. In Section 7, we will consider three probable causes: time variability of the shock parameters and particle acceleration, magnetic particle traps upstream, and the coordinate dependence of the shock angle.

5.2. Far-upstream Zone

To extend the fit shown in Figure 2 to the outermost part of the upstream plasma, we need to specify the parameters ψ and Ψ of the full solution in Equation (17). We argue below that these parameters are indeterminate within the given data set and should be treated as free model parameters. Nevertheless, they can be constrained within our model beyond the conditions $\Psi, \psi \ll F_0$, mentioned earlier.

First of all, they emerged as integration constants for a *steady-state* solution of the acceleration problem. If the steady state were absolute, we would be able to calculate the parameter Ψ using Equation (13): $\Psi = -(s - \sigma)F_0(\epsilon)/(s + 1)$. On the other hand, taking the (steady-state) DSA prediction at face value, we should expect $s = \sigma$, meaning $\Psi \to 0$ for sufficiently large ϵ where the injection from the thermal plasma core given by $Q(p)$ in Equation (8) fades out, irrespective of the seed particles for injection (Malkov & Drury 2001). Clearly, the $\Psi = 0$ condition constitutes an exact balance between the convective and diffusive particle fluxes in the shock precursor (see Equation (16)) resulting from the steady-state assumption. As we argued earlier, it is violated in a realistic time-dependent situation.

An indication of the time variability of the data provides an independently measured shock compression, r, yielding a steady-state DSA index $s = (r+2)/2(r-1)$ that does not match the index σ, directly obtained from the downstream spectrum. The shock compression ratio estimated in

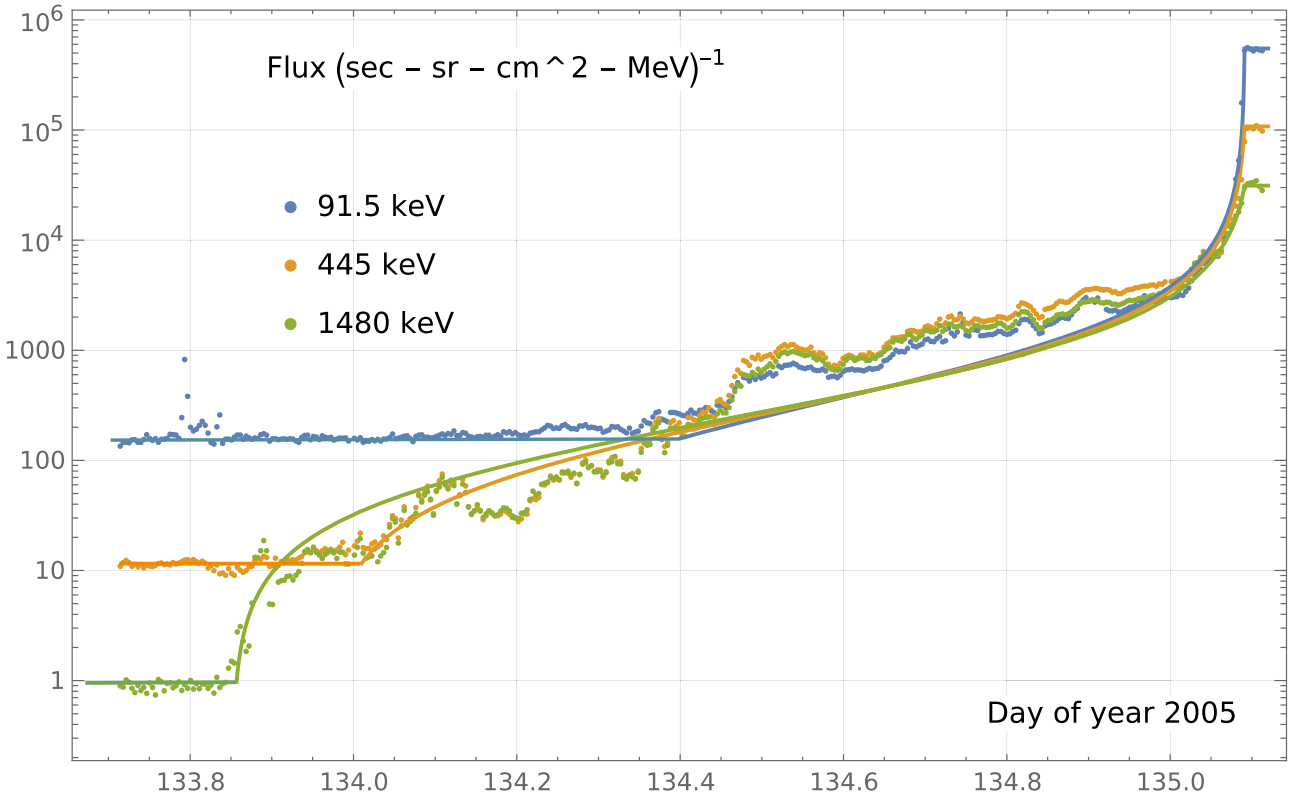

Figure 3. Fits in three energy channels produced using Equation (17) with parameters listed in Table 1.

Perri et al. (2023) in the range $2.4 < r < 3.6$ maps to the range of $s = 1.08-1.57$, whereas the measured downstream spectrum is outside of that range, $\sigma = 1.03$. As we mentioned, though, the shock may be modified by accelerated particles, which is visible in some observations, e.g., Terasawa (2011). Such a modification would increase the total shock compression between the far-upstream and downstream flow but decrease the shock compression at the flow discontinuity (Malkov & Drury 2001), often termed "subshock." Nevertheless, the flow modification would also violate the above relation between Ψ and F_0 because of a particle acceleration term, $\propto du/dz$, in the shock precursor.

Finally, the above relation between Ψ and F_0 is obtained by considering the flux balance at the shock transition. As we have seen, in the upstream region adjacent to the shock, the solution is not sensitive to Ψ, and a directly measured F_0 is sufficient to consistently describe the spectrum in the near- and mid-upstream areas. It then seems reasonable not to bind the constant Ψ to F_0 by the above relation, inferred from the solution near the shock, especially because Ψ significantly affects the solution on the opposite end of the flat spectrum, which is far upstream.

Similar arguments apply to ψ, introduced in Equation (7). The flux F varies by several orders of magnitude between the shock and far-upstream region, and only in the latter does ψ affect the result, while being negligible otherwise. Even the sign of ψ can be positive or negative depending on the relation between the background particle and wave energy density far upstream, just like in the case of Ψ. Some simple physical arguments are in order upon their signs.

Measured in the shock frame, the positive total particle flux Ψ in Equation (16) means that the shock-accelerated particles are transported away from it in the upstream direction, and their flux is predominantly diffusive. It also means that the accelerated particles are copiously injected at the shock instead of being accelerated out of the preexisting background population far upstream. The $\psi > 0$ condition, in turn, indicates that the background turbulence energy density far upstream dominates that of the energetic particles. The reverse arguments also apply in both instances. It seems that the only firm constraint that we can impose on these quantities is, indeed, Ψ, $\psi \ll F_0$.

That said, the sign of $\chi \equiv \Psi - \psi$ is crucial to the asymptotic spectra far upstream. From Equation (17), we deduce that $F \to -\psi$ for $\chi > 0$ and $F \to -\Psi$ for $\chi < 0$, when $\zeta|\chi| \to -\infty$. We can thus formally satisfy the boundary condition $F \to F_\infty(\epsilon)$ by choosing either the integration constant $\psi = -F_\infty$ or $\Psi = -F_\infty$, depending on whether $\chi = \Psi - \psi$ is positive or negative. These choices satisfy the boundary condition at $z = -\infty$, but approaching F_∞ is then gradual. We see from Figure 1, however, that $F(z)$ abruptly turns to an energy-dependent constant $F_\infty(\epsilon)$ at $z = -z_\infty(\epsilon)$. The spectrum ceases to be flat beyond this point. This abrupt transition requires the boundary condition $F(z \leqslant -z_\infty) = F_\infty$, with a break in the z-derivative at $z = -z_\infty$, as mentioned earlier. So, we have two input parameters, F_∞, z_∞, instead of one, F_∞. By extracting them for each particle energy from the data, we determine the two unknown parameters, Ψ and ψ, entering the full solution in Equation (17).

To summarize our spectrum fitting procedures, the normalized coordinate ζ contains the combination $\epsilon^{3/2}/\kappa_0(\epsilon)$ that we argued to be ϵ-independent. This is an accurate but not exact statement. We therefore introduce a weak power-law dependence of this quantity, $\propto \epsilon^{0.04}$, for a better agreement of the

breaking points, $z_\infty(\epsilon)$, in all energy channels. Likewise, we specify the functions $\Psi(\epsilon)$ and $\psi(\epsilon)$ as power-law functions. These quantities are defined by constant power-law indices (μ, γ, and ρ in Table 1). As we fit a continuum of profiles $F(\epsilon, z)$ using these three indices, the fine-tuning concerns do not apply. The fits are shown in Figure 3, and the required parameters are summarized in Table 1.

6. Conclusions

The following two modifications to the DSA theory suffice to explain spectral flattening observed ahead of several interplanetary shocks.

1. Inclusion of a dependence of particle diffusivity κ on the particle flux F (nonlinear particle transport) that, in turn, is directly related to the scattering wave intensity.
2. Switching from the traditional DSA resonant wave–particle interaction for short-scale magnetic perturbations that are also self-consistently generated by, but not resonant with, accelerated particles.

In the resulting DSA solution, the nonresonant, nonlinear particle diffusivity, κ, increases with energy as $\propto\epsilon^{3/2}$, simultaneously decreasing with the wave energy as $E_w^{-1} \propto \epsilon^{-3/2}F^{-1}$. As a result, κ does not explicitly depends on the particle energy almost everywhere in the shock precursor. This independence results in a diffusive flux $\propto F^{-1}\partial F/\partial z$ that being balanced with the convective flux, uF, results in an energy-independent $F(z)$ upstream.

7. Discussion

The presented acceleration model reproduces a surprisingly flat particle spectrum observed upstream of an interplanetary shock, including its transitions to a regular diffusively accelerated particle spectrum downstream and the inflowing background spectrum far upstream. Meanwhile, some spatial deviations of the flat part of the spectrum from the data remain. In part, they can be explained by variations in the shock angle entering the normalized coordinate ζ in Equation (15). However, their nonmonotonic parts cannot be accounted for within our steady-state model since the deviations are almost certainly time-dependent. This can be seen from the sign changes in the spatial gradient of the flux data upstream. If $\partial F/\partial z < 0$, both diffusive and convective fluxes are directed to the shock and cannot cancel out, thus precluding a steady-state solution in the shock frame. At the same time, nonmonotonic deviations from the predicted profile may constitute bunches of particles trapped in traveling magnetic disturbances. For example, they may result from magnetic perturbations driven by accelerated particles, subsequently steepening into shocklets or shock trains upstream (see, e.g., Kennel et al. 1988; Malkov & Diamond 2009 and references therein).

More broadly, magnetically trapped particles may originate from intrinsic shock instabilities, such as shock reformation and shock corrugations (Burgess et al. 2012; Caprioli & Spitkovsky 2014), that result in an impulsive release of accelerated particles upstream. They then propagate in bunches away from the shock. They may also be trapped in magnetic bubbles, self-created or preexisting in the solar wind. Since the accelerated particles near the shock upstream typically have an anisotropic distribution, they may drive mirror and firehose instabilities, resulting in magnetic bubbles that trap energetic particles. Consistent descriptions of their dynamics require a significant model extension, including a time-dependent shock description beyond one dimension. At this point, some additional DSA-unrelated acceleration of magnetically trapped particles upstream, e.g., second-order Fermi or magnetic pumping acceleration, cannot be ruled out.

The role of magnetic bubbles upstream and their interaction with energetic particles have already been discussed in an analysis of a 1978 interplanetary shock in Kennel et al. (1986). These authors presented a detailed data comparison with the Lee theory (Lee 1983), reaching a much closer agreement between the two than we found in the 2005 shock considered in the present paper. In particular, no spectrum flattening was observed in the 1978 shock, which is in complete agreement with Lee's predictions. The difference between the two shocks is that the 1978 shock has a significantly steeper downstream spectrum in the range $q = 4.20-4.25$, while the 2005 shock has $q \approx 4.06$, pointing to a considerably higher shock compression. However, the compression ratio estimate of Perri et al. (2023), $r \approx 3$, formally results in $q \approx 4.5$. The reason for this disagreement is, at least in part, that the above estimate of the shock compression has likely been obtained by analyzing the flow density and speed immediately upstream and downstream of the discontinuity. By inspecting these flow characteristics further upstream in Figure 1 of the above paper, one may see that the shock is significantly modified, most likely by accelerated particles penetrating upstream. The total compression is close to 4, consistent with the particle spectral index used in our paper.

Acknowledgments

This research work is supported by the NASA grant 80HQTR21T0005. M.M. gratefully acknowledges additional support from the NSF grant AST-2109103 and NASA ATP 80NSSC24K0774.

Appendix

Equation (6) can be derived as follows. Following Drury (1983), we can write the wave energy flux as $F_w = (u - V_A)E_w + uP_w$. In the absence of wave dissipation, this flux divergence, $\partial F_w/\partial z$, equates to the rate at which the wave pressure P_w does work against the gradient of energetic particles, $\partial P/\partial z$, which is $u\partial P_w/\partial z + V_A\partial P/\partial z$ (see Equations (4.41) and (4.46) in the above reference). After dividing both sides of this equality through V_A, Equation (6) follows.

ORCID iDs

Mikhail Malkov https://orcid.org/0000-0001-6360-1987
Joe Giacalone https://orcid.org/0000-0002-0850-4233
Fan Guo https://orcid.org/0000-0003-4315-3755

References

Axford, W. I., Leer, E., & Skadron, G. 1978, ICRC (Budapest), 11, 132
Bell, A. R. 1978, MNRAS, 182, 147
Bell, A. R. 2004, MNRAS, 353, 550
Bell, A. R., Matthews, J. H., & Blundell, K. M. 2019, MNRAS, 488, 2466
Blandford, R. D. 1980, ApJ, 238, 410
Blandford, R. D., & Ostriker, J. P. 1978, ApJL, 221, L29
Burgess, D., Möbius, E., & Scholer, M. 2012, SSRv, 173, 5
Bykov, A. M., Brandenburg, A., Malkov, M. A., & Osipov, S. M. 2013, SSRv, 178, 201

Caprioli, D., & Spitkovsky, A. 2014, ApJ, 783, 91
Diesing, R., & Caprioli, D. 2021, ApJ, 922, 1
Drury, L. O. 1983, RPPh, 46, 973
Drury, L. O. C., & Falle, S. A. E. G. 1986, MNRAS, 223, 353
Ellison, D. C., Moebius, E., & Paschmann, G. 1990, ApJ, 352, 376
Forman, M. A., & Webb, G. M. 1985, GMS, 34, 91
Hanusch, A., Liseykina, T. V., & Malkov, M. 2019, ApJ, 872, 108
Hanusch, A., Liseykina, T. V., Malkov, M. A., & Aharonian, F. A. 2019, ApJ, 885, 11
Iroshnikov, P. S. 1964, SvA, 7, 566
Kennel, C. F., Coroniti, F. V., Scarf, F. L., et al. 1986, JGR, 91, 11917
Kennel, C. F., Malkov, M. A., Sagdeev, R. Z., Shapiro, V. D., & Khrabrov, A. V. 1988, JETPL, 48, 79
Kraichnan, R. H. 1965, PhFl, 8, 1385
Krymskii, G. F. 1977, DoSSR, 234, 1306
Lario, D., Berger, L., Wilson, L. B. I., et al. 2018, JPhCS, 1100, 012014
Lario, D., Richardson, I. G., Wilson, L. B. W., III, et al. 2022, ApJ, 925, 198
Lee, M. A. 1982, JGR, 87, 5063
Lee, M. A. 1983, JGR, 88, 6109
Malkov, M. A., & Aharonian, F. A. 2019, ApJ, 881, 2
Malkov, M. A., & Diamond, P. H. 2009, ApJ, 692, 1571
Malkov, M. A., Diamond, P. H., & Sagdeev, R. Z. 2010, PPCF, 52, 124006
Malkov, M. A., & Drury, L. O. 2001, RPPh, 64, 429
Malkov, M. A., & Moskalenko, I. V. 2021, ApJ, 911, 151
Perri, S., Prete, G., Zimbardo, G., et al. 2023, ApJ, 950, 62
Skilling, J. 1975, MNRAS, 172, 557
Terasawa, T. 2011, in IAU Symp. 274, Advances in Plasma Astrophysics (Cambridge: Cambridge Univ. Press), 214
Völk, H. J., Drury, L. O., & McKenzie, J. F. 1984, A&A, 130, 19